

# Temperature Controls Guest Uptake and Release from $Zn_4L_4$ Tetrahedra

Dawei Zhang,<sup>†</sup> Tanya K. Ronson,<sup>†</sup> Songül Güryel,<sup>†</sup> John D. Thoburn,<sup>‡</sup> David J. Wales,<sup>†</sup> and Jonathan R. Nitschke<sup>\*,†</sup>

<sup>†</sup>Department of Chemistry, University of Cambridge, Lensfield Road, Cambridge CB2 1EW, United Kingdom

<sup>‡</sup>Department of Chemistry, Randolph-Macon College, Ashland, Virginia 23005, United States

## Supporting Information

**ABSTRACT:** We report the preparation of triazatruxene-faced tetrahedral cage **1**, which exhibits two diastereomeric configurations (T1 and T2) that differ in the handedness of the ligand faces relative to that of the octahedrally coordinated metal centers. At lower temperatures, T1 is favored, whereas T2 predominates at higher temperatures. Host–guest studies show that T1 binds small aliphatic guests, whereas T2 binds larger aromatic molecules, with these changes in binding preference resulting from differences in cavity size and degree of enclosure. Thus, by a change in temperature the cage system can be triggered to eject one bound guest and take up another.

Stimuli-responsive molecules<sup>1</sup> and molecular hosts<sup>2</sup> that are capable of adapting to changes in their environments have attracted substantial attention.<sup>3</sup> The ability of these species to switch between distinct states can enable them to be built into artificial molecular systems with useful functions.<sup>4</sup> One such function is the stimulus-controlled uptake and release of guests by molecular containers.<sup>5</sup> Such behavior has the potential to direct the outcome of chemical processes,<sup>4h,6</sup> control the transport and storage of chemicals,<sup>7</sup> and enable new means of drug delivery.<sup>8</sup>

Subcomponent self-assembled capsules are attractive candidates to achieve guest uptake and release, as the reversible formation of the dynamic covalent and coordinative bonds that hold the structures together provide different potential modes of opening.<sup>9</sup> Systems have thus been designed containing two or three capsules, where the application of chemical signals led to selective disassembly of individual cages and the release of their guests.<sup>10</sup> An alternative route for achieving guest uptake and release is the interconversion between supramolecular hosts with different guest preferences. However, these host transformations have been irreversible to date, in many cases resulting from the addition of new ligands<sup>11</sup> or templates.<sup>12</sup> Reversibility can be achieved in some cases by noninvasive stimuli, such as light,<sup>5c,13</sup> or by a change in solvent<sup>14</sup> or concentration,<sup>15</sup> enabling uptake and release of a single guest.

We hypothesized that stimuli-induced reconfiguration between two metal–organic hosts<sup>16</sup> with different guest preferences could lead to a system exhibiting switchable and reversible uptake and release of different guests. In this work, we demonstrate the functioning of such a system for the first

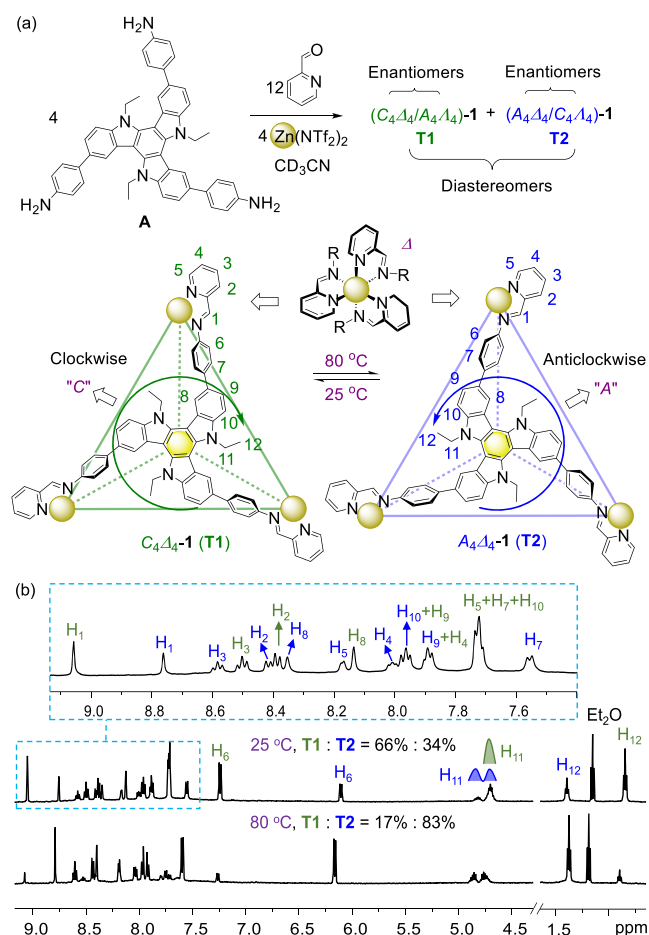


**Figure 1.** (a) Subcomponent self-assembly of **A** with 2-formylpyridine and  $Zn^{II}$  produced two diastereomeric pairs of enantiomers, as illustrated by the structures of  $C_4\Delta_4-1$  and  $A_4\Delta_4-1$ . (b)  $^1H$  NMR spectra ( $CD_3CN$ , 500 MHz) of **1** at 25 and 80 °C. The protons of  $(C_4\Delta_4/A_4\Delta_4)-1$  (T1) and  $(A_4\Delta_4/C_4\Delta_4)-1$  (T2) have been assigned and are indicated by green and blue labels, respectively.

time. Our system consists of a mixture of two thermally interconverting  $Zn_4L_4$  tetrahedral diastereomers (Figure 1).

Received: July 10, 2019

Published: September 3, 2019

Triazatruxene subcomponent **A** (4 equiv) reacted with 2-formylpyridine (12 equiv) and zinc(II) bis(trifluoromethanesulfonyl)imide (triflimide,  $\text{TF}_2\text{N}^-$ ) (4 equiv) in acetonitrile to give tetrahedron **1** (Figure 1a). The  $\text{Zn}_4\text{L}_4$  stoichiometry of the assembly was confirmed by ESI-MS (Figure S10). The triazatruxene moieties can be oriented either clockwise (*C*) or anticlockwise (*A*) within the faces of **1** (Figure 1a), and each trischelated octahedral vertex of the tetrahedron may adopt either  $\Lambda$  or  $\Delta$  handedness. The combination of these two stereochemical elements can thus produce diastereomers.<sup>17</sup> The  $^1\text{H}$  NMR spectrum of **1** exhibited two sets of ligand signals with the same DOSY diffusion coefficients (Figures 1b and S8), consistent with the presence of two distinct diastereomeric pairs of enantiomers, each belonging to the *T* point group, ( $\text{C}_4\Delta_4/\text{A}_4\Lambda_4$ )-**1** (**T1**) and ( $\text{A}_4\Delta_4/\text{C}_4\Lambda_4$ )-**1** (**T2**). In contrast, when iron(II) triflimide was used to produce an analogous tetrahedron from the same subcomponent precursors, only one of the two diastereomeric pairs was observed, exclusively ( $\text{A}_4\Delta_4/\text{C}_4\Lambda_4$ )- $\text{Fe}^{\text{II}}\text{L}_4$ .<sup>18</sup> Comparison of the  $^1\text{H}$  NMR spectral features of  $\text{Zn}_4\text{L}_4$  **1** and the previous  $\text{Fe}_4\text{L}_4$  structure, along with observations of their guest binding properties, allowed us to assign each of the two sets of signals in the  $^1\text{H}$  NMR spectrum of **1** to the corresponding isomer (see section 2.2 in the Supporting Information).

Density functional theory (DFT) calculations provided insight into the structural properties of the two diastereomers of **1**. The optimized structures showed that **T2** has larger pores between pairs of triazatruxene faces, rendering the tetrahedral framework more open than that of **T1**, as illustrated in Figure 2, and greatly increasing the void cavity size. Moreover, the

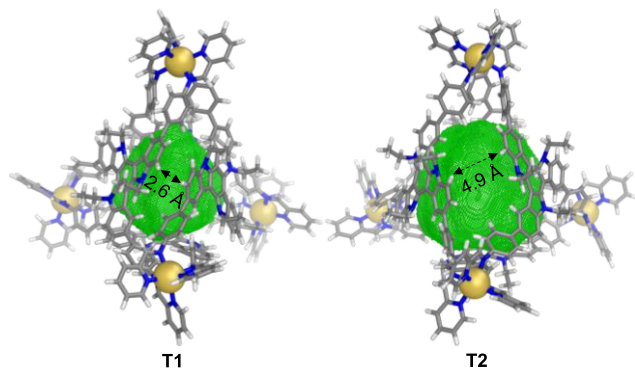


**Figure 2.** VOIDOO-calculated void spaces (green meshes) within the DFT-optimized models of  $\text{C}_4\Delta_4$ -**1** (**T1**) (volume = 423  $\text{\AA}^3$ ) and  $\text{A}_4\Delta_4$ -**1** (**T2**) (volume = 902  $\text{\AA}^3$ ) with all of the ethyl groups pointing outside of the cavities, viewed down a pore between two faces. Distances between the closest protons across adjacent faces are shown, highlighting the different degrees of cavity enclosure.

orientation of the ethyl groups on the triazatruxene faces of the tetrahedron, either toward or away from the center, was also found to affect the degree of enclosure, cavity volume, and cage stability (see section 4 in the Supporting Information).

The two cage isomers **T1** and **T2** were observed to interconvert in a temperature-dependent equilibrium (Figures 1 and S15). At 25  $^\circ\text{C}$ , a **T1**:**T2** ratio of 66:34 was observed, with **T1** predominating. The proportion of **T2** increased with temperature, leading to a **T1**:**T2** ratio of 17:83 at 80  $^\circ\text{C}$ . Re-equilibration back to the original proportions was observed after the mixture had been cooled back to 25  $^\circ\text{C}$  for 12 h. A van't Hoff analysis revealed **T1** to be enthalpically favorable

( $\Delta H = -8.51 \text{ kcal mol}^{-1}$ ), whereas **T2** is entropically favored ( $\Delta S = 2.73 \times 10^{-2} \text{ kcal K}^{-1} \text{ mol}^{-1}$ ) (Figure S16). Computation of the vibrational frequencies of the two structures also indicated the vibrational enhancement of the relative stability of **T2** versus **T1** with increased temperature (see section 4 in the Supporting Information), consistent with the experimental trend.

Cage **1** was first investigated as a host for smaller aliphatic guests. All of the guests shown in Figure 3a were observed to

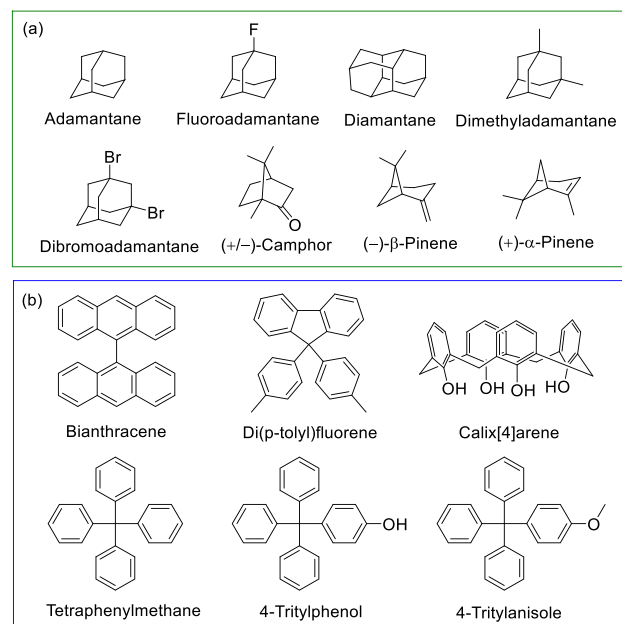


**Figure 3.** Guests investigated for **1**. (a) Smaller aliphatic guests and (b) larger aromatic guests were bound respectively by **T1** and **T2** in slow exchange on the NMR time scale at room temperature.

be encapsulated within **T1** in slow exchange on the NMR time scale at room temperature (Figures 4a and S22–S41). Titration of a guest into the host solution resulted in the appearance and increase in intensity of characteristically upfield-shifted signals for the bound guests in the range between  $-2.7$  and  $-0.6$  ppm, corresponding to 1:1 guest:**T1** complexes by  $^1\text{H}$  NMR integration. NOESY cross-peaks between the bound guest signals and the aromatic and methyl peaks of occupied **T1** were observed (see section 6.1 in the Supporting Information); no correlations were observed with those of **T2**. Slight shifts in the phenyl and methyl signals of **T2** ( $\text{H}_6$  and  $\text{H}_{12}$ ) were also observed in the presence of these guests, suggesting rapid guest exchange on the NMR time scale at room temperature. The presence of multiple equilibria in solution (Figure S21) prevented quantification of the binding strengths of these small guests.

Cage **1** was then investigated as a receptor for the larger guests bearing aromatic rings listed in Figure 3b. These guests were found to interact only with **T2** in slow exchange on the NMR time scale at room temperature (Figures 4b and S43–S61). Upon titration with each guest, new guest:**T2**  $^1\text{H}$  NMR signals were observed between 4.0 and 6.5 ppm, increasing in intensity as the guest was added. NOESY spectra exhibited cross-peaks between the signals of the bound guests and the aromatic protons of occupied **T2** (see section 6.2 in the Supporting Information); no such correlations were observed between signals from the guests shown in Figure 3b and those

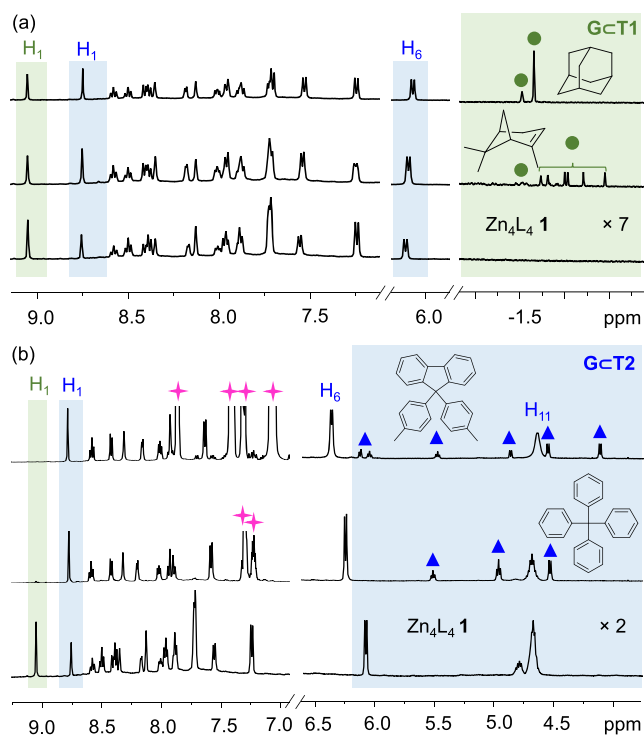


**Figure 4.**  $^1\text{H}$  NMR spectra ( $\text{CD}_3\text{CN}$ , 500 MHz, 25  $^\circ\text{C}$ ) of **1** in the presence of excess representative (a) aliphatic and (b) aromatic guests. Peak assignments are given in Figure 1. Green solid circles and blue solid triangles indicate the peaks of the guests bound in **T1** and **T2**, respectively. The peaks of the free aromatic guests in (b) are marked with magenta crosses.

of **T1**. Integration of the host–guest signals indicated a 1:1 binding stoichiometry in all cases. On the basis of  $^1\text{H}$  NMR titrations, the binding constants of **T2** for these larger guests were determined and showed a binding hierarchy of bianthracene > di(*p*-tolyl)fluorene > tetraphenylmethane > other guests (Table 1). We infer that both the abundance of aromatic rings and the three-dimensional structures of the guests play important roles in the favorable binding interactions.

**Table 1. Binding Constants of T2 for Large Aromatic Guests in  $\text{CD}_3\text{CN}$  at 25  $^\circ\text{C}$**

guest	$K_a$ ( $\text{M}^{-1}$ )
bianthracene	$(2.3 \pm 0.1) \times 10^5$
di( <i>p</i> -tolyl)fluorene	$(4.6 \pm 0.4) \times 10^4$
calix[4]arene	$(2.6 \pm 0.1) \times 10^3$
tetraphenylmethane	$(1.2 \pm 0.1) \times 10^4$
4-tritylphenol	$(1.7 \pm 0.2) \times 10^3$
4-tritylanisole	$(7.7 \pm 0.1) \times 10^3$

We noted that the addition of these guests also drove the equilibrium from **T1** to **T2** and that the presence of a large excess of guest resulted in the formation of the guestCT2 complex exclusively (Figure S43). The effect of guest binding on the equilibrium between **T1** and **T2** was investigated by considering the guest-induced change in the apparent Gibbs free energy difference ( $\Delta G'$ ) between the total concentrations of **T1** and **T2** (see section 6.2 in the Supporting Information). Our results showed that the progressive addition of each guest gradually switched the sign of  $\Delta G'$  from positive to negative

(Tables S7–S12), thus favoring species **T2** to a progressively greater degree by the end of the titration.

We infer that the different binding preferences of **T1** and **T2** derive from the differences in their cavity sizes and degrees of cavity enclosure. The smaller and more enclosed cavity of **T1** is more suitable for encapsulation of small aliphatic guests, in contrast to the larger and more open cavity of **T2** (Figure 2), which is better adapted to larger aromatic molecules.

We then explored the use of temperature to trigger the uptake and release of the different guests. Heating a mixture of **1** with one of the aliphatic guests listed in Figure 3a from 25 to 80  $^\circ\text{C}$  led to a significant decrease in the peak intensities of **T1** with a concomitant increase of those of **T2** (Figures S62–S69). The peaks of the bound guests within **T1** became nearly undetectable at 80  $^\circ\text{C}$ , indicating the release of these guests from **T1**. Cooling the mixture back to 25  $^\circ\text{C}$  for 2 days regenerated the initial ratio of **T1** and **T2**, leading to reuptake of the released guests by **T1**. For instance, the equilibrium mixture of **1** and dibromoadamantane contained 50% and 9% guestCT1 at 25 and 80  $^\circ\text{C}$ , respectively (Table S13). Switching the temperature thus enabled the reversible uptake and release of dibromoadamantane from **T1** due to the 41% change in the population of guestCT1.

In contrast, heating a mixture of **1** and one of the aromatic guests listed in Figure 3b increased the population of guestCT2 (Figures S70–S73) because of the greater thermodynamic stability of **T2** at higher temperatures, which drove the uptake of the guest. Re-equilibration of the mixture at 25  $^\circ\text{C}$  for 2 days led to a decrease in the **T2** population and the release of the **T2**-bound guest. This process is exemplified by the case of calix[4]arene, which showed a 15% change in the population of guestCT2, switching between 24% and 39% when the temperature was changed between 25 and 80  $^\circ\text{C}$ , leading to the reversible uptake and release of calix[4]arene from **T2** (Table S14). It should be noted that the temperature-dependent capture and release by **T2** is impracticable in the presence of a large excess of an aromatic guest from Figure 3b because of the complete formation of guestCT2 even at 25  $^\circ\text{C}$ , as discussed above (Figure S43).

We then investigated the simultaneous uptake and release of a pair of different guests, dibromoadamantane (**G1**) and calix[4]arene (**G2**), within a single system (Figure 5). The initial equilibrium mixture at 25  $^\circ\text{C}$  contained **G1CT1** as the major species (52%), relative to the populations of **G2CT2** (16%) and empty **T1** and **T2** (32% in total) (Figure S74 and Table S18). This hierarchy was inverted at 80  $^\circ\text{C}$ , with only 3% **G1CT1** and 50% **G2CT2**. The temperature increase thus

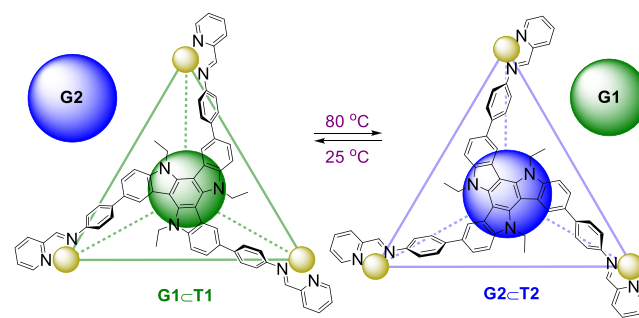


**Figure 5.** Schematic representation of reversible uptake and release of the guests dibromoadamantane (**G1**) and calix[4]arene (**G2**) by **T1** and **T2**, respectively, via thermoswitching.

resulted in the release of **G1** from **T1** and the uptake of **G2** by **T2**. Conversely, the release of **G2** from **T2** and the uptake of **G1** by **T1** occurred as the initial equilibrium population was re-established when the mixture re-equilibrated at 25 °C over 2 days.

In summary, a new and straightforward means of stimulus-directed guest uptake and release has been developed that is based upon the different thermodynamic stabilities of the two diastereomers of tetrahedral host **1** and their differential guest preferences. This ability to reversibly catch and release guests may prove useful in the context of new switchable catalytic systems, where a catalyst is released only when needed, or in new modes of chemical purification, where a cargo molecule may be selectively taken up from a mixture, moved to where it is needed, and released in pure form following a temperature change.

## ■ ASSOCIATED CONTENT

### ■ Supporting Information

The Supporting Information is available free of charge on the ACS Publications website at DOI: 10.1021/jacs.9b07307.

Complete experimental details (PDF)

## ■ AUTHOR INFORMATION

### Corresponding Author

\*jrn34@cam.ac.uk

### ORCID

David J. Wales: 0000-0002-3555-6645

Jonathan R. Nitschke: 0000-0002-4060-5122

### Notes

The authors declare no competing financial interest.

## ■ ACKNOWLEDGMENTS

This work was supported by the European Research Council (695009) and the UK Engineering and Physical Sciences Research Council (EPSRC EP/M008258/1). The authors thank the Department of Chemistry NMR Facility at the University of Cambridge for performing some NMR experiments and the EPSRC UK National Mass Spectrometry Facility at Swansea University for carrying out high-resolution mass spectrometry. D.Z. acknowledges a Herchel Smith Research Fellowship from the University of Cambridge. J.D.T. acknowledges the Rashkind Family Endowment and the Cheney Endowment from Randolph-Macon College.

## ■ REFERENCES

(1) (a) Gavette, J. V.; Mills, N. S.; Zakharov, L. N.; Johnson, C. A., 2nd; Johnson, D. W.; Haley, M. M. An anion-modulated three-way supramolecular switch that selectively binds dihydrogen phosphate,  $\text{H}_2\text{PO}_4^-$ . *Angew. Chem., Int. Ed.* **2013**, *52*, 10270–10274. (b) Aprahamian, I. Hydrazone switches and things in between. *Chem. Commun.* **2017**, *53*, 6674–6684. (c) Russew, M. M.; Hecht, S. Photoswitches: from molecules to materials. *Adv. Mater.* **2010**, *22*, 3348–3360. (d) Zhuang, J.; Gordon, M. R.; Ventura, J.; Li, L.; Thayumanavan, S. Multi-stimuli responsive macromolecules and their assemblies. *Chem. Soc. Rev.* **2013**, *42*, 7421–7435. (e) Ma, X.; Tian, H. Stimuli-responsive supramolecular polymers in aqueous solution. *Acc. Chem. Res.* **2014**, *47*, 1971–1981. (f) Xue, M.; Yang, Y.; Chi, X.; Yan, X.; Huang, F. Development of pseudorotaxanes and rotaxanes: from synthesis to stimuli-responsive motions to applications. *Chem. Rev.* **2015**, *115*, 7398–7501. (g) Wu, N. M.; Ng, M.; Lam, W. H.; Wong, H. L.; Yam, V. W. Photochromic heterocycle-fused thieno[3,2-b]phosphole oxides as visible light switches without sacrificing

photoswitching efficiency. *J. Am. Chem. Soc.* **2017**, *139*, 15142–15150.

(2) (a) Frischmann, P. D.; MacLachlan, M. J. Metallocavitands: an emerging class of functional multimetallic host molecules. *Chem. Soc. Rev.* **2013**, *42*, 871–890. (b) Hasell, T.; Cooper, A. I. Porous organic cages: soluble, modular and molecular pores. *Nat. Rev. Mater.* **2016**, *1*, 16053. (c) Custelcean, R. Anion encapsulation and dynamics in self-assembled coordination cages. *Chem. Soc. Rev.* **2014**, *43*, 1813–1824. (d) Diaz-Moscoso, A.; Ballester, P. Light-responsive molecular containers. *Chem. Commun.* **2017**, *53*, 4635–4652. (e) Zhang, Z.; Kim, D. S.; Lin, C. Y.; Zhang, H.; Lammer, A. D.; Lynch, V. M.; Popov, I.; Miljanic, O. S.; Anslyn, E. V.; Sessler, J. L. Expanded porphyrin-anion supramolecular assemblies: environmentally responsive sensors for organic solvents and anions. *J. Am. Chem. Soc.* **2015**, *137*, 7769–7774.

(3) (a) Yang, H.; Yuan, B.; Zhang, X.; Scherman, O. A. Supramolecular chemistry at interfaces: host-guest interactions for fabricating multifunctional biointerfaces. *Acc. Chem. Res.* **2014**, *47*, 2106–2115. (b) McConnell, A. J.; Wood, C. S.; Neelakandan, P. P.; Nitschke, J. R. Stimuli-responsive metal-ligand assemblies. *Chem. Rev.* **2015**, *115*, 7729–7793. (c) Zhiquan, L.; Xie, H.; Border, S. E.; Gallucci, J.; Pavlovic, R. Z.; Badjic, J. D. A Stimuli-responsive molecular capsule with switchable dynamics, chirality, and encapsulation characteristics. *J. Am. Chem. Soc.* **2018**, *140*, 11091–11100. (d) Zhang, M.; Yan, X.; Huang, F.; Niu, Z.; Gibson, H. W. Stimuli-responsive host-guest systems based on the recognition of cryptands by organic guests. *Acc. Chem. Res.* **2014**, *47*, 1995–2005. (e) Cohen, E.; Soffer, Y.; Weissman, H.; Bendikov, T.; Schilt, Y.; Raviv, U.; Rybtchinski, B. Hydrophobicity control in adaptive crystalline assemblies. *Angew. Chem., Int. Ed.* **2018**, *57*, 8871–8874. (f) De Poli, M.; Zawodny, W.; Quinonero, O.; Lorch, M.; Webb, S. J.; Clayden, J. Conformational photoswitching of a synthetic peptide foldamer bound within a phospholipid bilayer. *Science* **2016**, *352*, 575–580. (g) Kim, S.; Castillo, H. D.; Lee, M.; Mortensen, R. D.; Tait, S. L.; Lee, D. From foldable open chains to shape-persistent macrocycles: synthesis, impact on 2D ordering, and stimulated self-assembly. *J. Am. Chem. Soc.* **2018**, *140*, 4726–4735. (h) Dal Molin, M.; Verolet, Q.; Colom, A.; Letrun, R.; Derivery, E.; Gonzalez-Gaitan, M.; Vauthey, E.; Roux, A.; Sakai, N.; Matile, S. Fluorescent flippers for mechanosensitive membrane probes. *J. Am. Chem. Soc.* **2015**, *137*, 568–571.

(4) (a) Feringa, B. L. The art of building small: from molecular switches to motors (Nobel Lecture). *Angew. Chem., Int. Ed.* **2017**, *56*, 11060–11078. (b) Natali, M.; Giordani, S. Molecular switches as photocontrollable “smart” receptors. *Chem. Soc. Rev.* **2012**, *41*, 4010–4029. (c) Stoddart, J. F. Mechanically interlocked molecules (MIMs)-molecular shuttles, switches, and machines (Nobel Lecture). *Angew. Chem., Int. Ed.* **2017**, *56*, 11094–11125. (d) Sauvage, J. P. From chemical topology to molecular machines (Nobel Lecture). *Angew. Chem., Int. Ed.* **2017**, *56*, 11080–11093. (e) Kassem, S.; van Leeuwen, T.; Lubbe, A. S.; Wilson, M. R.; Feringa, B. L.; Leigh, D. A. Artificial molecular motors. *Chem. Soc. Rev.* **2017**, *46*, 2592–2621. (f) Erbas-Cakmak, S.; Leigh, D. A.; McTernan, C. T.; Nussbaumer, A. L. Artificial molecular machines. *Chem. Rev.* **2015**, *115*, 10081–10206. (g) Lee, S.; Flood, A. H. Photoresponsive receptors for binding and releasing anions. *J. Phys. Org. Chem.* **2013**, *26*, 79–86. (h) Biswas, P. K.; Saha, S.; Paululat, T.; Schmittel, M. Rotating catalysts are superior: suppressing product inhibition by anchimeric assistance in four-component catalytic machinery. *J. Am. Chem. Soc.* **2018**, *140*, 9038–9041. (i) Nielsen, K. A.; Sarova, G. H.; Martin-Gomis, L.; Stein, P. C.; Sanguinet, L.; Levillain, E.; Sessler, J. L.; Guldi, D. M.; Sastre-Santos, A.; Jeppesen, J. O. Chloride anion controlled molecular “switching”. Binding of 2,5,7-trinitro-9-dicyanomethylene-fluorene- $\text{C}_{60}$  by tetra-thiafulvalene calix[4]pyrrole and photophysical generation of two different charge-separated states. *J. Am. Chem. Soc.* **2008**, *130*, 460–462. (j) Wang, H.; Liu, F.; Helgeson, R. C.; Houk, K. N. Reversible photochemically gated transformation of a hemicarcerand to a carcerand. *Angew. Chem., Int. Ed.* **2013**, *52*, 655–659. (k) Kim, T. Y.; Vasdev, R. A. S.; Preston, D.; Crowley, J. D. Strategies for

reversible guest uptake and release from metallocsupramolecular architectures. *Chem. - Eur. J.* **2018**, *24*, 14878–14890.

(5) (a) Kishi, N.; Akita, M.; Kamiya, M.; Hayashi, S.; Hsu, H. F.; Yoshizawa, M. Facile catch and release of fullerenes using a photoresponsive molecular tube. *J. Am. Chem. Soc.* **2013**, *135*, 12976–12979. (b) Dube, H.; Ajami, D.; Rebek, J., Jr. Photochemical control of reversible encapsulation. *Angew. Chem., Int. Ed.* **2010**, *49*, 3192–3195. (c) Han, M.; Michel, R.; He, B.; Chen, Y. S.; Stalke, D.; John, M.; Clever, G. H. Light-triggered guest uptake and release by a photochromic coordination cage. *Angew. Chem., Int. Ed.* **2013**, *52*, 1319–1323. (d) Preston, D.; Fox-Charles, A.; Lo, W. K.; Crowley, J. D. Chloride triggered reversible switching from a metallocsupramolecular  $[Pd_2L_4]^{4+}$  cage to a  $[Pd_2L_2Cl_4]$  metallo-macrocyclic with release of endo- and exo-hedrally bound guests. *Chem. Commun.* **2015**, *51*, 9042–9045. (e) Samanta, S. K.; Quigley, J.; Vinciguerra, B.; Briken, V.; Isaacs, L. Cucurbit[7]uril Enables Multi-stimuli-responsive release from the self-assembled hydrophobic phase of a metal organic polyhedron. *J. Am. Chem. Soc.* **2017**, *139*, 9066–9074. (f) Zhang, D.; Cochrane, J. R.; Di Pietro, S.; Guy, L.; Gornitzka, H.; Dutasta, J. P.; Martinez, A. Breathing<sup>o</sup> motion of a modulable molecular cavity. *Chem. - Eur. J.* **2017**, *23*, 6495–6498.

(6) Galli, M.; Lewis, J. E.; Goldup, S. M. A Stimuli-responsive rotaxane-gold catalyst: regulation of activity and diastereoselectivity. *Angew. Chem., Int. Ed.* **2015**, *54*, 13545–13549.

(7) (a) Saywell, A.; Bakker, A.; Mielke, J.; Kumagai, T.; Wolf, M.; Garcia-Lopez, V.; Chiang, P. T.; Tour, J. M.; Grill, L. Light-induced translation of motorized molecules on a surface. *ACS Nano* **2016**, *10*, 10945–10952. (b) Chen, J.; Wezenberg, S. J.; Feringa, B. L. Intramolecular transport of small-molecule cargo in a nanoscale device operated by light. *Chem. Commun.* **2016**, *52*, 6765–6768. (c) Shanmugaraju, S.; Umadevi, D.; Savyasachi, A. J.; Byrne, K.; Ruether, M.; Schmitt, W.; Watson, G. W.; Gunnlaugsson, T. Reversible adsorption and storage of secondary explosives from water using a Tröger's base-functionalised polymer. *J. Mater. Chem. A* **2017**, *5*, 25014–25024.

(8) (a) Cullen, W.; Turega, S.; Hunter, C. A.; Ward, M. D. pH-dependent binding of guests in the cavity of a polyhedral coordination cage: reversible uptake and release of drug molecules. *Chem. Sci.* **2015**, *6*, 625–631. (b) Mura, S.; Nicolas, J.; Couvreur, P. Stimuli-responsive nanocarriers for drug delivery. *Nat. Mater.* **2013**, *12*, 991. (c) Giglio, V.; Varela-Aramburu, S.; Travaglini, L.; Fiorini, F.; Seeberger, P. H.; Maggini, L.; De Cola, L. Reshaping silica particles: Mesoporous nanodiscs for bimodal delivery and improved cellular uptake. *Chem. Eng. J.* **2018**, *340*, 148–154. (d) Ding, C.; Tong, L.; Feng, J.; Fu, J. Recent advances in stimuli-responsive release function drug delivery systems for tumor treatment. *Molecules* **2016**, *21*, 1715.

(9) Zhang, D.; Ronson, T. K.; Nitschke, J. R. Functional capsules via subcomponent self-assembly. *Acc. Chem. Res.* **2018**, *51*, 2423–2436.

(10) (a) McConnell, A. J.; Aitchison, C. M.; Grommet, A. B.; Nitschke, J. R. Subcomponent exchange transforms an  $Fe^{II}_4L_4$  cage from high- to low-spin, switching guest release in a two-stage system. *J. Am. Chem. Soc.* **2017**, *139*, 6294–6297. (b) Castilla, A. M.; Ronson, T. K.; Nitschke, J. R. Sequence-dependent guest release triggered by orthogonal chemical signals. *J. Am. Chem. Soc.* **2016**, *138*, 2342–2351. (c) Jimenez, A.; Bilbeisi, R. A.; Ronson, T. K.; Zarra, S.; Woodhead, C.; Nitschke, J. R. Selective encapsulation and sequential release of guests within a self-sorting mixture of three tetrahedral cages. *Angew. Chem., Int. Ed.* **2014**, *53*, 4556–4560.

(11) (a) Zheng, Y. R.; Lan, W. J.; Wang, M.; Cook, T. R.; Stang, P. J. Designed post-self-assembly structural and functional modifications of a truncated tetrahedron. *J. Am. Chem. Soc.* **2011**, *133*, 17045–17055. (b) Zhou, X. P.; Wu, Y.; Li, D. Polyhedral metal-imidazolate cages: control of self-assembly and cage to cage transformation. *J. Am. Chem. Soc.* **2013**, *135*, 16062–16065. (c) Li, J.-R.; Zhou, H.-C. Bridging-ligand-substitution strategy for the preparation of metal–organic polyhedra. *Nat. Chem.* **2010**, *2*, 893. (d) Bhat, I. A.; Samanta, D.; Mukherjee, P. S. A Pd<sub>24</sub> Pregnant molecular nanoball: self-templated stellation by precise mapping of coordination sites. *J. Am. Chem. Soc.* **2015**, *137*, 9497–9502.

(12) (a) Sekiya, R.; Fukuda, M.; Kuroda, R. Anion-directed formation and degradation of an interlocked metallohelicate. *J. Am. Chem. Soc.* **2012**, *134*, 10987–10997. (b) Scherer, M.; Caulder, D. L.; Johnson, D. W.; Raymond, K. N. Triple helicate—tetrahedral cluster interconversion controlled by host-guest interactions. *Angew. Chem., Int. Ed.* **1999**, *38*, 1587–1592. (c) Lee, H.; Elumalai, P.; Singh, N.; Kim, H.; Lee, S. U.; Chi, K. W. Selective synthesis of ruthenium(II) Metalla[2]catenane via solvent and guest-dependent self-assembly. *J. Am. Chem. Soc.* **2015**, *137*, 4674–4677. (d) Chifotides, H. T.; Giles, I. D.; Dunbar, K. R. Supramolecular architectures with  $\pi$ -acidic 3,6-bis(2-pyridyl)-1,2,4,5-tetrazine cavities: role of anion- $\pi$  interactions in the remarkable stability of Fe(II) metallacycles in solution. *J. Am. Chem. Soc.* **2013**, *135*, 3039–3055.

(13) (a) Chen, S.; Chen, L. J.; Yang, H. B.; Tian, H.; Zhu, W. Light-triggered reversible supramolecular transformations of multi-bisthiethylene hexagons. *J. Am. Chem. Soc.* **2012**, *134*, 13596–13599. (b) Oldknow, S.; Martir, D. R.; Pritchard, V. E.; Blitz, M. A.; Fishwick, C. W. G.; Zysman-Colman, E.; Hardie, M. J. Structure-switching  $M_3L_2$  Ir(III) coordination cages with photo-isomerising azo-aromatic linkers. *Chem. Sci.* **2018**, *9*, 8150–8159.

(14) (a) Heo, J.; Jeon, Y. M.; Mirkin, C. A. Reversible interconversion of homochiral triangular macrocycles and helical coordination polymers. *J. Am. Chem. Soc.* **2007**, *129*, 7712–7713. (b) Baxter, P. N. W.; Khoury, R. G.; Lehn, J.-M.; Baum, G.; Fenske, D. Adaptive self-assembly: environment-induced formation and reversible switching of polynuclear metalocyclophanes. *Chem. - Eur. J.* **2000**, *6*, 4140–4148. (c) Kilbas, B.; Mirtschin, S.; Scopelliti, R.; Severin, K. A solvent-responsive coordination cage. *Chem. Sci.* **2012**, *3*, 701–704. (d) Fujita, M.; Ibukuro, F.; Hagihara, H.; Ogura, K. Quantitative self-assembly of a [2]catenane from two preformed molecular rings. *Nature* **1994**, *367*, 720. (e) Gidron, O.; Jirasek, M.; Trapp, N.; Ebert, M. O.; Zhang, X.; Diederich, F. Homochiral [2]catenane and bis[2]catenane from alleno-acetylenic helicates - a highly selective narcissistic self-sorting process. *J. Am. Chem. Soc.* **2015**, *137*, 12502–12505.

(15) (a) Frischmann, P. D.; Kunz, V.; Stepanenko, V.; Wurthner, F. Subcomponent self-assembly of a 4 nm  $M_4L_6$  tetrahedron with Zn(II) vertices and perylene bisimide dye edges. *Chem. - Eur. J.* **2015**, *21*, 2766–2769. (b) Weilandt, T.; Troff, R. W.; Saxell, H.; Rissanen, K.; Schalley, C. A. Metallo-supramolecular self-assembly: the case of triangle-square equilibria. *Inorg. Chem.* **2008**, *47*, 7588–7598. (c) Lu, X.; Li, X.; Guo, K.; Xie, T. Z.; Moorefield, C. N.; Wesdemiotis, C.; Newkome, G. R. Probing a hidden world of molecular self-assembly: concentration-dependent, three-dimensional supramolecular interconversions. *J. Am. Chem. Soc.* **2014**, *136*, 18149–18155. (d) Yamamoto, T.; Arif, A. M.; Stang, P. J. Dynamic equilibrium of a supramolecular dimeric rhomboid and trimeric hexagon and determination of its thermodynamic constants. *J. Am. Chem. Soc.* **2003**, *125*, 12309–12317.

(16) Wang, W.; Wang, Y. X.; Yang, H. B. Supramolecular transformations within discrete coordination-driven supramolecular architectures. *Chem. Soc. Rev.* **2016**, *45*, 2656–2693.

(17) (a) Wang, X.; Wang, Y.; Yang, H.; Fang, H.; Chen, R.; Sun, Y.; Zheng, N.; Tan, K.; Lu, X.; Tian, Z.; Cao, X. Assembled molecular face-rotating polyhedra to transfer chirality from two to three dimensions. *Nat. Commun.* **2016**, *7*, 12469. (b) Wang, Y.; Fang, H.; Tranca, I.; Qu, H.; Wang, X.; Markvoort, A. J.; Tian, Z.; Cao, X. Elucidation of the origin of chiral amplification in discrete molecular polyhedra. *Nat. Commun.* **2018**, *9*, 488.

(18) Zhang, D.; Ronson, T. K.; Greenfield, J. L.; Brotin, T.; Berthault, P.; Leonce, E.; Zhu, J. L.; Xu, L.; Nitschke, J. R. Enantiopure  $[Cs^+/XeCcryptophane]CFe^{II}_4L_4$  hierarchical superstructures. *J. Am. Chem. Soc.* **2019**, *141*, 8339–8345.